Co-Hyperpolarized Dehydroascorbate and Pyruvate MRI Predicts Radiation Response in Glioblastoma Models

Authors

Elizabeth Coffee[1,2], Paola Porcari[3†], Saket Patel[3†], Grace Figlioli[3], Marjan Berishaj[3], Ingo K. Mellinghoff[1,4], Kayvan R. Keshari[3,5,6]

1. Department of Neurology, Memorial Sloan Kettering Cancer Center, New York, NY
2. Department of Neurology, Weill Cornell Medicine, New York, NY
3. Department of Radiology, Memorial Sloan Kettering Cancer Center, New York, NY, USA.
4. Human Oncology and Pathogenesis Program, Memorial Sloan Kettering Cancer Center, New York, NY
5. Molecular Pharmacology Program, Memorial Sloan Kettering Cancer Center, New York, NY
6. Gerstner Sloan Kettering School for Biomedical Sciences, Memorial Sloan Kettering Cancer Center, New York, NY 10065, USA

† These authors contributed equally to this work.

Running title. Predicting GBM response using an oxidative stress MRI probe.

Corresponding Author: Kayvan R. Keshari, PhD. rahimikk@mskcc.org. 417 E 68th St., New York, NY 10065

Conflict of Interest: K.R.K. is a founders of Atish Technologies and a member of the scientific advisory boards of Nvision Imaging Technologies, Imaginostics and Mi2. K.R.K. hold patents related to imaging and modulation of cellular metabolism. I.K.M is a member of advisory board for Agios Pharmaceuticals, Inc., Black Diamond Therapeutics, Voyager Therapeutics, Inc., Prelude Therapeutics, Novartis, F. Homann-La Roche, and is site-PI for clinical trials sponsored by Eli Lilly, Kazia Therapeutics Limited, Erasca, and Servier Pharmaceuticals LLC. E.C is co-PI for a trial sponsored by Telix Pharmaceuticals Inc.

Other authors declare no potential conflicts of interest.

Word Count: 4927

Figures: 5

Supplementary files: 4

Significance:

This study introduces hyperpolarized DHA/pyruvate MRI as a noninvasive biomarker enabling real-time quantification of oxidative stress to predict glioblastoma radiation response before conventional imaging detects treatment effects.

Abstract

Glioblastoma (GBM) remains the most aggressive and treatment-resistant primary malignant brain tumor in adults. Current imaging assessments fail to capture early metabolic responses to therapy, underscoring the need for biomarkers that reflect treatment efficacy in real time. Radiation critical component of GBM treatment, increasing oxidative stress on the cell through numerous mechanisms. This study investigates metabolic reprogramming in response to oxidative stress as an indicator of radiosensitivity and evaluates co-hyperpolarized (HP) [1-^{13}C] dehydroascorbate and [1-^{13}C] pyruvate (HP DHA/PA) magnetic resonance imaging as a quantitative approach to assess redox and glycolytic flux changes in GBM. *In vitro* analyses across four human GBM cell lines revealed that glutathione depletion sensitizes some GBM cells to radiation, with corresponding upregulation of the pentose phosphate pathway (PPP) and pyrimidine synthesis. Leveraging both radiosensitive and radioresistant orthotopic xenograft GBMs, co-hyperpolarized DHA/PA imaging detected reductions in both DHA-to-vitamin C and pyruvate-to-lactate conversion in radiosensitive tumors *in vivo*, reflecting diminished reductive capacity and oxidative stress following radiation. Metabolomic profiling confirmed increased pyrimidine metabolism in responsive tumors and purine metabolism in resistant ones, aligning with known mechanisms of radioresistance. Collectively, these findings establish HP DHA/PA imaging as the first non-invasive method to quantify oxidative stress and identify radiation responders in GBM prior to anatomical changes.

I. Introduction

Glioblastoma is most common primary malignant brain tumor in adults, and the most resistant to treatment. Despite aggressive multimodality treatment, median overall survival of 12-15 months remains effectively unchanged since the implementation of standard of care chemoradiation after maximal safe resection two decades ago.(1) A major limitation to the advancement of the field is our inability to assess treatment response in real time. Current response assessments are limited to visualization of anatomic stability on contrasted magnetic resonance imaging (MRI), a process that requires months of surveillance. MRI changes from treatment effects (pseudoprogression) or antiangiogenic therapy (pseudoresponse) complicate interpretation of these assessments. There is, therefore, a distinct unmet clinical need for improved biomarkers for treatment response in glioblastoma.

One avenue to assess treatment response is to quantify oxidative stress, a hallmark effect of ionizing radiation treatment. Beyond radiation, sensitivity to the standard-of-care treatment temozolomide has been linked to increased reactive oxygen species (ROS)(2) and numerous compounds that impact cellular redox balance are under investigation.(3) While many modalities for probing regionally specific oxidative stress are being developed, there are no clinically available methods to quantify this component of tumor metabolism.

Molecular imaging is the minimally invasive probing of biological processes at the cellular and molecular level and is being increasingly utilized to address the need for earlier read outs of treatment response. Hyperpolarized (HP) MRI one such molecular imaging method that increases the lifespan and visibility of endogenous substrates, and when paired with carbon labeling magnetic resonance spectroscopy, permits the real-time quantification of metabolic reactions in vivo.(4) Hyperpolarized [1-^{13}C] pyruvate is the most commonly utilized HP MRI imaging probe with > 60 published human studies.(5) Beyond pyruvate, HP [1-^{13}C] dehydroascorbate has been utilized as a redox sensor in preclinical studies to quantify oxidative stress in a variety of disease states.(6-14)

We present the use of co-hyperpolarized dehydroascorbate and pyruvate (HP DHA/PA) to predict treatment response to radiation in orthotopic models of glioblastoma. We first assess the variable radiosensitivity in four human glioblastoma cell lines and characterize the metabolic response to radiation in vitro, highlighting dependence on antioxidant availability and upregulation of pyrimidine synthesis. We then develop an imaging method for probing this process in vivo highlighting differences between nucleotide metabolism in radiosensitive and radioresistant GBMs. Lastly, we identify a biomarker for treatment response in vivo models of glioblastoma with promising clinical applications.

II. Methods

Cell culture: Human U87-MG, A172, T98 human male glioblastoma cell lines (American Type Culture Collection, Manassas, VA, United States) and U251 glioblastoma cell line (gift from the laboratory of Ingo Mellinghoff and authenticated via STR analysis October 2025), were used. Cells were cultured in Dulbecco's modified Eagle's medium without glucose, supplemented with 10% fetal bovine serum (Gibco BRL, Thermo Fisher Scientific), penicillin (50 U/ml) and streptomycin (250 µg/ml; Gibco), and 5.5 mM glucose in a humidified 5% CO_2/95% air at 37°C.

Cells were tested for mycoplasma using MycoAlert® Mycoplasma Detection Kit Unless (Lonza LT07-318) every 2 months and used only at low passage (<10) for all experiments. Unless otherwise noted, cells were cultured in 5.5 mM glucose media to reflect physiologic conditions.

Radiation response in vivo: Radiation for all experiments was administered via X-ray irradiator XRAD-320 at a rate 117 cGy/min. Viability assays were performed by counting viable cells after trypsinization and resuspension 72 hours after treatment. cells treated with L-Buthionine-(S,R)-Sulfoximine (Cayman Chemical, 14484), cells were treated with 500uM BSO for 18 hours preceding radiation (or sham irradiation) treatment unless otherwise noted. Proliferation assays were performed on IncuCyte SX5 (Sartorious) and confluence at 72 hours was normalized to starting confluence per well before normalizing to untreated control. All experiments were performed in biologic triplicates.

Colony Forming Assay: CFA were performed by plating 1000 cells in a 6-well plate. Wells were treated with 100uM BSO for 18 hours, 10 Gy radiation, or both and maintained in high glucose DMEM (25 mM). After 14 days, cells were fixed with 4% paraformaldehyde and stained with 0.1% crystal violet. Colonies containing > 50 cells were counted manually.

Carbon Tracing: Cells were treated with 5 mM [1,2-13C] glucose (Sigma 453188) in DMEM without glucose and media collected after 4 hours. Media samples were prepared with a standard media buffer solution, 5mM ^{13}-C urea for concentration analysis, and 2uL of gavodvist in 500 uL solution and run in a ^{13}C NMR at 600 MHz (Avance III). NMR data were processed using the Mnova Software Suite (version 14.3.2, Santiago de Compostela, Spain). Lactate signals centered at 20.1 ppm were normalized to 1-^{13}C urea at 160ppm, and line fitting within Mnova used to calculate integral under each peak.

Metabolomics: GBM cells (triplicate for each condition) or tumor samples (n=3 mice for each of 4 conditions, 12 total) were mixed or homogenized in cold (−80 °C) 80% methanol. After centrifuging, samples were normalized and lyophilized by speed vac. Dried pellets were resuspended in 1:1 methanol:H2O before LC-MS/MS analysis. Metabolites were separated by Hydrophilic interaction chromatography (HILIC) and detected by high-resolution mass spec (5ppm mass accuracy). Samples were run in triplicate on a Vanquish Horizon / Q-Exactive HF Orbitrap LC-MS system. Untargeted metabolite profiling of cell and tissue extracts was performed first using definitive identification based on the mass and retention time of authentic chemical standards, followed by putatively annotated compounds by searching HMDB database using accurate mass. MetaboAnalyst 6.0 was used for data processing. Raw intensities were normalized to median and log2 transformed. Pathway enrichment analysis was conducted first by selecting metabolites using a threshold of $p<0.05$ and FC > 2 and Q-stat based on established methods(15), run against a library of SMPDB based on normal human metabolic pathways. Pathways enriched with $p> 0.1$ were included. Individual metabolite pool values were compared using normalized data before log transformation. Volcano plots for tumor samples were generated using thresholds of $p<0.1$ and FC >1.5 (<0.66) in tumor samples due to a wide variability in sample intensities after normalization. Raw data is included as a supplementary file.

Orthotopic Xenografts: All animal studies were done in accordance with IACUC approved protocol. Immortalized human glioblastoma cells were orthotopically implanted in athymic

Foxn1nu mice (Jackson Laboratories). Anesthetized mice were placed into a stereotaxic frame (Stoelting Co., Wood Dale, IL, United States), and 3×10^5 cells in suspension were injected in a volume of 2 µl of phosphate-buffered saline via a stereotaxic injector at a flow rate of 2 µl/min into the right striatum of the mice (coordinates from bregma: 0.0-mm posterior, 2.5-mm lateral, and 3.0-mm ventral).

Spectroscopic Imaging: To investigate whether HP DHA/PA could reveal distinct metabolic profiles of radioresistant and radiosensitive tumors, four groups of athymic nude mice (Jackson Laboratories) were imaged (n=3 of each U251 and U251 RT, n=4 of each U87 and U87 RT). Mice underwent tail vein cannulation and were anesthetized using isoflurane. Spectroscopic imaging experiments were performed on a Bruker BioSpec 3.0-T/18-cm horizontal bore system (Bruker BioSpin, Billerica, MA, United States). A dual-tuned 1H/^{13}C transmit/receive radio frequency volume coil (Bruker BioSpin MRI GmbH, Ettlingen, Germany) was used. Multislice T2-weighted fast spin echo (TSE) images of mouse brain were acquired in the coronal orientation as an anatomical reference [repetition time (TR)/effective echo time (TEeff) = 2500/33 ms)]. Static magnetic field homogeneity was optimized using a localized field-map shimming routine (ParaVision 360, v2.0 pl 1, Bruker BioSpin).

After initial imaging sequences, anesthesia was held before injection with the HP solution. Each mouse underwent the ^{13}C hyperpolarized MRI scan 15 s after injecting 150 µl of co-hyperpolarized 40 mM [1-^{13}C]DHA, 90 mM [1-^{13}C]pyruvate over 10 seconds. 2D multivoxel CSI sequence was acquired coronally (TR/TE_{eff} = 141.4/5 ms, field of view = 32 × 32 mm^2, flip angle of 20°, in-plane resolution of 2.667 × 2.667 mm^2, 5 mm slice thickness centered over the brain tumor). The ^{13}C CSI sequence was repeated on a cylindrical ^{13}C urea phantom (6M) for signal normalization.

Hyperpolarized Data analysis: Spectroscopic data were preprocessed through a custom Matlab script (Matlab R2021b, The MathWorks) applying 10 Hz apodization, zero-filling interpolation (ZFP), baseline correction. Processed spectra were then overlayed on coronal T2-weighted image of the mouse brain in Spectroscopic Imaging, Visualization and Computing (Sivic 0.9) software package.(16) ROIs were selected over the tumor and contralateral brain (CLB). Integration regions selected for each of: Pyruvate, DHA, Vitamin C, Pyruvate Hydrate, and Lactate. For each experiment, the mean values of each quantified metabolite per ROI was determined and normalized to the 6 M ^{13}C urea phantom imaged in the same experiment. Measured polarization and concentrations of injected substrates were used to determine the normalized concentration of each metabolite.

Tissue extraction: Mice were sacrificed utilizing isoflurane overdose in accordance with IACUC approved animal protocol. Mouse brains were rapidly extracted under cold condition and were snap frozen either whole or after tumor dissection in liquid nitrogen. Whole brain samples for tissue staining were sectioned at -20C using a cryostat in 10 µm slices. Immunohistochemistry with Ki-67 (CST #D2H10) Rabbit mAb (CST #9027) at 2 µL/ml was performed. Immunofluorescence was performed with with Anti-gamma H2A.X (phospho S139) antibody (Abcam #11174) and Alexa Fluor 594.

Statistical Analysis: Data analyses were performed using GraphPad Prism. A two-tailed paired or unpaired Student's t test was used to determine significance when two conditions were

compared and is noted in the text. For experiments with more than two conditions a one or two-way ANOVA was used. For survival data a log rank test was used. In all cases values of $p < 0.05$ were considered significant. $p < 0.05$; **, $p < 0.01$; ***, $p < 0.001$; ****, $p < 0.0001$. Data are shown as mean ± SEM (standard error of the mean).

III. Results

A. Glutathione Depletion Increases Glioblastoma Sensitivity to Radiation

To investigate differences in response to radiation, we examined four immortalized glioblastoma cell lines. First, we examined viability at 72 hours after treatment with ascending doses of ionizing radiation: 0 Gy, 2 Gy, 4 Gy, and 10 Gy (Fig 1A) to estimate an IC50 for each cell line. T98s exhibited the highest resistance to treatment (IC50=7.2 Gy, R^2=0.75). At the cellular level, the equilibrium between reductive and oxidative electron transfer reactions is critical for maintaining cellular functions. Reduced glutathione (GSH) is a the most abundant neutralizer of reactive oxygen species (ROS) and its' balance with oxidized glutathione (GSSG) is a marker of cellular oxidative stress.(17) Radiation causes dysregulation of cellular redox status and oxidative stress via the formation of free radicals which impacts downstream signaling pathways, leading to changes in cell growth, differentiation, and cell death.(18) We therefore examined the effects of glutathione depletion on the sensitivity to radiation in glioblastoma cell lines (Fig 1B-E). Buthionine sulfoximine (BSO) is a potent irreversible inhibitor the rate-limiting enzymatic reaction in glutathione synthesis driven by gamma-glutamylcysteine synthetase (γ-GCS) that has been shown to increase sensitivity to radiation.(19) We assessed proliferation in each cell line at 72 hours after treatment with radiation and 500uM BSO. Treatment with 10 Gy caused a decrease in proliferation in all 4 cell lines, whereas a glutathione depletion with a sublethal dose of BSO further sensitized only U87 and U251 to radiation (Fig1B). Radiation induced oxidative stress and double stranded DNA breaks induce cell-cycle arrest, senescence or cell death from multiple mechanisms including apoptosis, necrosis, ferroptosis and others.(18) In the case of apoptosis, PARP (poly[ADP-ribose] polymerase) is a nuclear enzyme that detects DNA strand breaks and facilitates base excision repair by catalyzing the transfer of ADP-ribose units from NAD+ to target proteins.(20) To assess apoptotic cell death, we probed cleaved-PARP in the cell lines radiosensitized with glutathione depletion 48 hours after treatment (Fig1C) and saw that only U251s underwent increased apoptosis in response to radiation and glutathione depletion whereas U87s did not, suggesting an alternate mechanism of cell death.

Proliferative potential was examined using clonogenic assays, an established in vitro assay for determining effects of treatment on adherent cell proliferative integrity by monitoring a single cell's ability to proliferate. We noted all lines exhibited diminished proliferative potential after exposure to 100uM BSO for 18 hours or 10 Gy (Fig 1D). Further, the compound effect of radiation with glutathione depletion seen at 72 hours in U87 and U251 was recapitulated at 2 weeks, reinforcing the impact of glutathione depletion on radiation response in those GBM lines.

B. Radiation Response in Glioblastoma is Characterized by Increase in Nucleotide Metabolism

The metabolic response to DNA damage is an upregulation of the Pentose Phosphate Pathway (PPP) to produce ribose-5-phosphate for nucleotide synthesis and NADPH which combats

oxidative stress.(21) To assess immediate metabolic changes in response to radiation, we quantified the flux through the PPP using [1,2 -^{13}C] labeled glucose given immediately after radiation and measured extracellular lactate production. Glycolysis primarily produces [2-^{13}C2] lactate ((M+2) isotopomer), while the PPP, followed by glycolysis, generates [3-^{13}C] lactate ((M+1) isotopomer).(22) We measured both the rate of PPP activity and the ratio of singlet (M+1)lactate to doublet(M+2) lactate to estimate PPP/glycolysis flux. All four GBM lines increased PPP flux (Fig 2A) and the PPP/Glycolysis ratio (Fig 2B) in response to radiation, however only U87 and U251s increased PPP flux in response to glutathione depletion. In both lines, pretreatment with BSO increased the radiation induced upregulation of PPP flux and PPP/Glycolytic flux.

To further investigate the metabolic effects of radiation on glioblastoma cells in vitro, untargeted metabolomics (LC-MS) 48 hours after radiation was performed on cell extracts of U87 and U251 cells. Pathway overexpression enrichment analysis (Fig 2C-D) revealed U87s and U251s exposed to radiation both enriched pathways of pyrimidine metabolism (p=0.006 and p=0.0004, respectively) and purine metabolism (p=0.015 and p=0.043, respectively). In U87s, PPP was also enriched (p=0.006). As expected in response to increased oxidative stress, metabolite pool size analysis (E-H) revealed glutathione was significantly decreased in both GBM lines exposed to radiation when compared to untreated controls (E), however only U251s exhibited an imbalance in GSH/GSSG oxidative stress balance, suggesting a unique vulnerability to oxidative stress. Both lines had increased pool sizes of 6-PG, a key intermediate in oxidative PPP which supports both nucleotide synthesis and oxidative stress resistance (G). Decrements in lactate generation after radiation were seen in both GBM lines (H) and supporting prior work on this topic.(23,24) Since the last step of anaerobic glycolysis reduces pyruvate to lactate depends on NADH, the activation of PARP and resultant depletion of NAD+ drives competition for NAD(H) availability, contributing to lower lactate as previously described in lymphoma tumors treated with etoposide.(25)

Taken together, we demonstrate the metabolic and proliferative responses to radiation are impacted by glutathione availability. Relatively radiosensitive glioblastoma cells in vitro upregulate pentose phosphate pathway and nucleotide synthesis and decrease lactate production.

C. U251 are more radiosensitive than U87 orthotopic xenografts in vivo

To investigate the metabolic consequences of radiation *in vivo*, we selected U251 and U87 lines for orthotopic xenograft implantation. Tumor sizes were measured twice weekly after stereotactic injection via MRI using T_2-weighted imaging. Images in the coronal plane were used to measure tumor area using ROI segmentation in each slice and multiplied by the slice thickness to estimate tumor volume. Mice were treated with 0Gy (control) or 8Gy whole brain radiation in one dose 1-3 days after tumor detection on MRI. Mice were monitored for weight and neurologic morbidity and sacrificed at pre-determined thresholds for each. Tumor volumes were plotted from day of tumor detection to remove the variability with tumor engraftment rate, and mice who did not develop tumors were excluded from analysis. Tumor volume curves demonstrate a similar rate of growth between untreated U251s and U87s. Radiation slows the growth of both tumor types, though much more pronounced in U251s. Further, all of the radiated U251s decreased in size in response to radiation (Fig 3A). Survival analyses demonstrated a median overall survival benefit of 9 days in U87s treated with radiation when compared to untreated controls (U87 mOS = 12 days, U87 RT mOS = 21 days) and a median overall survival benefit of 17.5 days in mice with U251s treated

with radiation (U251 mOS = 14 days, U251 RT mOS = 31.5 days) (Long Rank for all groups: X^2=14.52, p <0.0001) when compared with untreated controls (Fig 3B). In a separate cohort of mice, representative brains from each group were extracted and flash frozen 48 hours after 0Gy or 8Gy radiation. A modest qualitative decrease in proliferation was seen in radiosensitive U251s treated with radiation, alongside an increase in ds-DNA damage and apoptosis (Ki-67 and γ-H2AX respectively, Figure 3D), which were not seen in radioresistant U87s. Cleaved-PARP expression was increased in both tumor types 48 hours after radiation (Fig 3C).

D. Decrements in Oxidative Stress and Glycolytic Flux Predict Response to Radiation in Glioblastoma

Based on the demonstrated sensitivity to glutathione availability and decrement in lactate production in the response to radiation, we hypothesized that probing reductive capabilities of tumors would reveal early metabolic effects of radiation. To accomplish this, we utilized co-hyperpolarized [1-^{13}C] dehydroascorbic acid and [1-^{13}C] pyruvic acid. Dehydroascorbic acid (DHA) is readily transported across the blood-brain barrier and enters the cell through GLUT1 where it is rapidly two-electron reduced to Vitamin C (Vit C) in a glutathione and NADPH dependent reaction. Hyperpolarized (HP) [1-^{13}C] DHA, therefore, can be used to assess the capacity of tumors to resist oxidative stress. HP DHA has demonstrated ability to act as a redox sensor in multiple preclinical models(7,8,10) including prostate cancer.(6) We have developed co-polarized DHA with pyruvic acid, the most widely used HP imaging probe. HP Pyruvate enables real time assessment of glycolytic flux via quantification of lactate generation (among other products), which has been studied clinically in tumor diagnosis, predicting tumor grade, and treatment response in brain, breast, renal, and prostate cancer. (26-29) Combining HP DHA with HP PA, unique chemical shifts allow us to spatially resolve both substrates and their respective products (lactate and Vitamin C) using spectroscopic imaging (Fig 4A). We utilized a 2D chemical shift imaging (CSI) in the coronal plane for this study.

We first compared the spatial differences in brain metabolism in mice bearing U251 or U87 brain tumors (Fig 4B) compared to the contralateral brain (CLB). Using methods we have previously published,(12) absolute concentrations of each metabolite were calculated. There was no difference in substrate perfusion in either tumor type (Supplementary 1), however U87s did demonstrate increased lactate production, which is expected due to increased anaerobic glycolysis in cancer, known as the Warburg Effect (Lactate/Total Carbon difference of 0.12, p = 0.09). U251 tumors did not generate more lactate at baseline than the corresponding CLB, and neither tumor type generated a difference in Vitamin C from DHA.

Radiosensitive U251 tumors treated with radiation led to decrement in the conversion of DHA to Vit C and in pyruvates conversion to lactate when compared to untreated controls, reflective of diminished reductive capacity of these tumors after treatment (Fig 4C). Correspondingly, radioresistant U87 tumors demonstrated no difference in relative lactate or Vit C generation after radiation, reflecting maintenance of their reductive capacity in the face of oxidative stress. We investigated the product of Lactate/Total Carbon and Vit C /(DHA + Vit C) as a combined readout to capture the activity of both pathways simultaneously, and found it was likewise significantly

lower in radiosensitive U251 tumors, highlighting its potential use as a single biomarker for treatment response (Fig 4D).

E. Glioblastomas Responding to Radiation Increase Pyrimidine Metabolism

To identify global metabolic changes that would dictate the observed metabolic imaging phentopyes *in vivo*, we performed unlabeled non-targeted Liquid Chromatography-Mass Spectrometry (LC-MS) analysis of mouse brain metabolome from flash frozen athymic nude mice brains with tumors (n=3 for each group). We examined relative abundance (Log2 fold change) and statistical significance (-Log10 (P-value)) of radiated tumors versus their untreated controls of the same tumor type (Fig 5A-B). Radiosensitive U251s demonstrated significant increases in pyrimidine intermediate UDP and thymine in response to radiation (Fig 5B) which was expected based on our in vitro pathway enrichment analysis (Fig 2D). However, radioresistant U87s *in vivo* demonstrated a different phenotype and metabolic profile than *in vitro*, with a decrement in pyrimidine metabolism intermediate UDP (U87RT/U87 FC=0.46, p=0.01) and a modest but significant increase in core purine base (FC=1.16, p=0.06) (Fig 5A). Pool sizes of select metabolites further support the upregulation of pyrimidine metabolism in radiosensitive tumors and purine metabolism in radioresistant tumors (Fig 5D).

IV. Discussion

We present the first study utilizing HP DHA as a redox sensor in brain tumor models and demonstrate the quantification of oxidative stress using HP DHA/PA as a tool to identify treatment response in glioblastoma before anatomic changes can be seen. We show that radiation treatment is characterized by upregulating pyrimidine synthesis via PPP flux in response to increased oxidative stress in glioblastoma, and leverage glutathione dependence as an indicator of reductive capacity to identify treatment responders in vivo.

Mechanisms of cell death after radiation can include apoptosis, necrosis, ferroptosis, and mitotic catastrophe.(30) Timely assessments of radiosensitivity in vitro are limited by high levels of resistance in glioblastoma tumor cells. In our work, assessments of viability were more sensitive than proliferation assessments in the 3 days following radiation. U87s lack cleaved-PARP 48 hours after radiation, which suggest that these cells undergo an alternate mechanism of cell death *in vitro* besides caspase-mediated apoptosis.

The metabolic response to radiation is characterized by increase in PPP flux, generating both nucleotide precursors to repair DNA damage and NADPH as a reducing agent to combat intracellular oxidative stress.(31) Our in vitro data are concordant with this paradigm. Cellular response to radiation in these four GBM lines was characterized by increase in PPP rate and relative flux when compared to glycolysis explaining the decrement in lactate generation seen in pool size analysis. NADPH is a product of driving PPP forward, supporting the need for antioxidants in response to radiation induced oxidative stress. Along with NADPH and NADH, reduced glutathione (GSH) is another key antioxidant that maintains cellular redox homeostasis. Decreased glutathione pool sizes seen in both radiated cell lines is consistent with the consumption of reducing agents in response to oxidative stress. Further, we demonstrate that

glioblastoma sensitivity to radiation is augmented by glutathione depletion, reinforcing the potential utility of a redox sensor to measure radiation response.

Phenotypic differences in the response to radiation in U87s emphasize the importance of *in vivo* studies in this group. Physiologic variables associated with in vivo tumors including the tumor microenvironment, perfusion, impact of immunogenicity, methodologic techniques such as the time to extraction and contamination with nearby brain tissue, and low sample sizes likely contributed to the higher variance seen in tissue metabolomics data compared to in vitro. More liberal significance cutoffs for p-value (>0.1) and fold change (<0.5 and >1.5) were used to elucidate metabolic trends, though the generalizability of these findings remains to be seen. Despite this variability, trends in metabolic phenotypes complement the existing literature.

Inhibition of de novo pyrimidine synthesis has been investigated clinically in cancers with disappointing results.(32) However, a newly targeted intermediate in this pathway has been recently exploited as a therapeutic vulnerability in brain cancers(33,34) by targeting dihydroorotate dehydrogenase (DHODH), a key intermediate in the synthesis of uridine monophosphate (UMP), a precursor for thymidine and cytosine. Shi et al. demonstrated IDH-mutant (IDHmt) tumors were more vulnerable to the imbalance of pyrimidines and purines induced by DHODH inhibition than IDH-wild type,(35) and Pal et. al. showed that adult-type glioblastoma, which is IDH wild-type by definition (IDHwt), was not as vulnerable to DHODH inhibition as diffuse midline glioma.(36) Together, these studies suggest that GBMs may be less dependent on pyrimidine synthesis upregulation. In line with this, our data demonstrated that only relatively radiosensitive adult-type glioblastoma U251s (IDHwt) upregulated pyrimidine synthesis in response to radiation. Clinically, glioblastomas are inherently resistant to treatment, so we hypothesize this immortalized cell line may exhibit phenotypic behavior more similar to tumor types which are therapeutically vulnerable to inhibition to pyrimidine synthesis.

In contrast to the radiosensitive U251s, the relatively radioresistant U87s did not demonstrate this same upregulation in pyrimidine synthesis in vivo, and in fact seemed to favor purine metabolism with a significant decrement in UDP and trending increase in purine bases and inosine. In a metabolomic study of 23 glioblastoma cell lines, Zhou et. al. correlated increases in purine metabolism with radioresistance and demonstrated the inhibition of guanosine triphosphate (GTP) synthesis via the rate limiting enzyme inosine monophosphate dehydrogenase (IMPDH1) specifically sensitizes radioresistant GBM models to radiation, including U87s.(37) They went on correlate lower IMPDH1 gene expression with poorer prognosis in The Cancer Genome Atlas Database, a finding which was validated in two other large international cancer genomic databases.(38) Our work strengthens the metabolic dependence on purine metabolism in radioresistant glioblastoma.

Hyperpolarized [1-^{13}C] pyruvate is being clinically investigated as a tool to predict treatment response in a variety of cancer indications. The basis of these investigations is founded in the Warburg effect, in which cancer cells preferentially convert pyruvate to lactate even in the presence of functioning mitochondria and oxidative phosphorylation. Thus, quantifying this reaction has been shown to predict tumor grade, distinguish tumor from nontumor tissue, and

identify treatment responders.(26-28,39) The NADH dependent conversion of pyruvate to lactate catalyzed by LDH serves as a marker both for glycolytic flux and an indirect quantification of NADH availability. We utilize co-polarization with [1-^{13}C] dehydroascorbate, which undergoes rapid NADPH and glutathione dependent reduction to Vitamin C. Thus, the availability of reducing agents (GSH, NADPH, and NADH) can be detected by quantifying the conversion of pyruvate to lactate and DHA to Vit C. Given known induction of oxidative stress by ionizing radiation, the influence of glutathione availability on radiation response *in vitro*, and decrement in lactate production after treatment, we identified HP DHA/PA as an ideal imaging biomarker to quantify the response to radiation and identify treatment responders before anatomic changes could be visualized.

2D-Chemical Shift Imaging after injection with HP DHA/PA revealed a decrement in lactate and Vitamin C production in radiosensitive U251. This is contrary to findings in a previous study utilizing hyperpolarized pyruvate which did not detect a difference in lactate production in orthotopic models of U251s treated with radiation,(40) which may be due to a lower dose of radiation (6Gy compared to 8Gy in our study) or to evaluation at an earlier time point. Mair et. al. quantified lactate generation using HP pyruvate at baseline and in response to radiation in U87 tumors along with four patient derived xenografts, revealing correlation of lactate labeling with c-Myc expression and glycolytic enzyme expression (LDHA, HK2) which were associated with radioresistance of cell lines in vitro.(41) Increased lactate generation at baseline in radioresistant U87s when compared to contralateral brain in our study is consistent with this framework, and maintenance of high generation of lactate after radiation suggests resistance to treatment. Likewise, a decrement in lactate production is consistent with tumors that are responding to treatment, as was seen in radiosensitive U251s in our study. Our work, taken together with existing literature, support the utility of longitudinal monitoring of metabolic profiles before and after treatment to monitor the tumor metabolic response to treatment over time.

Given the role of oxidative stress in a plethora of human diseases, the development of a non-toxic, spatially resolved and quantitative oxidative stress imaging biomarker is an unmet clinical need that would greatly improve our ability to tailor patient treatment plans. Methods to image oxidative stress *in vivo* include fluorescent probes which are difficult to implement *in vivo* and paramagnetic MRI contrast agents which are often limited by short relaxation times.(42) Radiolabeling of fluorescent probes and radiolabeled imaging of downstream consequences of oxidative stress have been utilized in PET but come at the cost of radiation exposure. Prior work by our group and others utilizing HP DHA have demonstrated utility of this endogenous substrate as a redox sensor in models of a variety of malignancies including lymphoma,(13) colorectal cancer,(14) and prostate cancer(6) along with nonmalignant disease states.(7,8,11) Recently, co-polarized HP DHA/PA was shown to achieve high enough spatial resolution to distinguish distinct regional metabolic profiles between white matter and deep gray nuclei in the mouse brain.(12)

Our data show that in a state of oxidative stress, both lactate and Vit C generation will decrease in response to a bolus of their substrates. Combining these readouts provides a singular variable reflective of the overall reductive capacity of the tumor and could be used as a biomarker for treatment response. We therefore propose examining the product of lactate/total carbon and Vit C / (DHA + Vit C) as a unified parameter reflective of the overall state of oxidative stress. It is

possible that there are conditions in which only one of Vit C or Lactate goes down, or both decrease but only modestly. Combining these variables is expected to be more sensitive than considering each product individually and should reflect the overall reductive capacity of the tumor, simplifying the interpretation of the results. Future studies with co-polarized substrates could employ similar tactics, strengthening the clinical translatability of new HP imaging probes.

We present the first study successfully quantifying oxidative stress in glioblastoma models using hyperpolarized molecular imaging. Further, we identify a singular biomarker, Lactate X Vitamin C, with the ability to predict radiation response before anatomic changes can be visualized. Beyond applications in radiation response, a variety of other cancer-directed therapeutics are aimed at targeting oxidative stress(3), broadening the potential applications of HP DHA beyond radiation response in this population. HP DHA/PA, therefore, holds potential to transform our ability to monitor treatment response in brain tumors in real time. Future studies to assess utility in treatment response monitoring in patient-derived xenograft models will strengthen preclinical biologic validation and lay the groundwork for successful clinical translation in this population.

V. Acknowledgements:
We acknowledge all Keshari lab members for help with experiments or preparation of this manuscript. We thank the MSKCC cores for their help in designing and conducting experiments: Antitumor Assessment core, Molecular Cytology core, NMR Analytical core and the Animal Imaging core. Mass spectrometric analyses were performed at the Weill Cornell Medicine Proteomics and Metabolomics Core Facility. This work was supported by the National Institute of Health – P30 CA008748, R01 CA252037 (K.R.K), The Paul Calabresi Career Development Award for Clinical Oncology: K12 CA184746, and the MSK Imaging and Radiation Sciences Program (IMRAS) Seed Grant.

Contributions

Conceptualization, K.R.K., I.K.M; methodology, K.R.K., E.C., P.P., S. P.; investigation E.C., P.P., S. P. G.F., M. B.; formal analysis, E.C., K.R.K.; writing-original draft: E.C.; writing—review and editing, E.C., P.P., S. P.; supervision, K.R.K., I.K.M; funding acquisition K.R.K. and E.C.

Data Availability Statement: Data were generated by the authors and included in the article**.**

References

1. Stupp R, Mason WP, van den Bent MJ, Weller M, Fisher B, Taphoorn MJ*, et al*. Radiotherapy plus concomitant and adjuvant temozolomide for glioblastoma. N Engl J Med 2005;352(10):987-96 doi 10.1056/NEJMoa043330.
2. Lo Dico A, Salvatore D, Martelli C, Ronchi D, Diceglie C, Lucignani G*, et al*. Intracellular Redox-Balance Involvement in Temozolomide Resistance-Related Molecular Mechanisms in Glioblastoma. Cells 2019;8(11) doi 10.3390/cells8111315.
3. Liu S, Dong L, Shi W, Zheng Z, Liu Z, Meng L*, et al*. Potential targets and treatments affect oxidative stress in gliomas: An overview of molecular mechanisms. Front Pharmacol 2022;13:921070 doi 10.3389/fphar.2022.921070.
4. Miloushev VZ, Keshari KR, Holodny AI. Hyperpolarization MRI: Preclinical Models and Potential Applications in Neuroradiology. Top Magn Reson Imaging 2016;25(1):31-7 doi 10.1097/RMR.0000000000000076.
5. Larson PEZ, Bernard JML, Bankson JA, Bogh N, Bok RA, Chen AP*, et al*. Current methods for hyperpolarized [1-(13)C]pyruvate MRI human studies. Magn Reson Med 2024;91(6):2204-28 doi 10.1002/mrm.29875.
6. Keshari KR, Sai V, Wang ZJ, Vanbrocklin HF, Kurhanewicz J, Wilson DM. Hyperpolarized [1-13C]dehydroascorbate MR spectroscopy in a murine model of prostate cancer: comparison with 18F-FDG PET. J Nucl Med 2013;54(6):922-8 doi 10.2967/jnumed.112.115402.
7. Keshari KR, Wilson DM, Sai V, Bok R, Jen KY, Larson P*, et al*. Noninvasive in vivo imaging of diabetes-induced renal oxidative stress and response to therapy using hyperpolarized 13C dehydroascorbate magnetic resonance. Diabetes 2015;64(2):344-52 doi 10.2337/db13-1829.
8. Wilson DM, Di Gialleonardo V, Wang ZJ, Carroll V, Von Morze C, Taylor A*, et al*. Hyperpolarized (13)C Spectroscopic Evaluation of Oxidative Stress in a Rodent Model of Steatohepatitis. Sci Rep 2017;7:46014 doi 10.1038/srep46014.
9. Keshari KR, Kurhanewicz J, Bok R, Larson PE, Vigneron DB, Wilson DM. Hyperpolarized 13C dehydroascorbate as an endogenous redox sensor for in vivo metabolic imaging. Proc Natl Acad Sci U S A 2011;108(46):18606-11 doi 10.1073/pnas.1106920108.
10. Qin H, Carroll VN, Sriram R, Villanueva-Meyer JE, von Morze C, Wang ZJ*, et al*. Imaging glutathione depletion in the rat brain using ascorbate-derived hyperpolarized MR and PET probes. Sci Rep 2018;8(1):7928 doi 10.1038/s41598-018-26296-6.
11. Baligand C, Qin H, True-Yasaki A, Gordon JW, von Morze C, Santos JD*, et al*. Hyperpolarized (13) C magnetic resonance evaluation of renal ischemia reperfusion injury in a murine model. NMR Biomed 2017;30(10) doi 10.1002/nbm.3765.
12. Patel S, Porcari P, Coffee E, Kim N, Berishaj M, Peyear T*, et al*. Simultaneous noninvasive quantification of redox and downstream glycolytic fluxes reveals compartmentalized brain metabolism. Sci Adv 2024;10(51):eadr2058 doi 10.1126/sciadv.adr2058.
13. Bohndiek SE, Kettunen MI, Hu DE, Kennedy BW, Boren J, Gallagher FA*, et al*. Hyperpolarized [1-13C]-ascorbic and dehydroascorbic acid: vitamin C as a probe for

imaging redox status in vivo. J Am Chem Soc 2011;133(30):11795-801 doi 10.1021/ja2045925.
14. Timm KN, Hu DE, Williams M, Wright AJ, Kettunen MI, Kennedy BWC*, et al*. Assessing Oxidative Stress in Tumors by Measuring the Rate of Hyperpolarized [1-13C]Dehydroascorbic Acid Reduction Using 13C Magnetic Resonance Spectroscopy. J Biol Chem 2017;292(5):1737-48 doi 10.1074/jbc.M116.761536.
15. Goeman JJ, van de Geer SA, de Kort F, van Houwelingen HC. A global test for groups of genes: testing association with a clinical outcome. Bioinformatics 2004;20(1):93-9 doi 10.1093/bioinformatics/btg382.
16. Crane JC, Olson MP, Nelson SJ. SIVIC: Open-Source, Standards-Based Software for DICOM MR Spectroscopy Workflows. Int J Biomed Imaging 2013;2013:169526 doi 10.1155/2013/169526.
17. Monostori P, Wittmann G, Karg E, Turi S. Determination of glutathione and glutathione disulfide in biological samples: an in-depth review. J Chromatogr B Analyt Technol Biomed Life Sci 2009;877(28):3331-46 doi 10.1016/j.jchromb.2009.06.016.
18. Jiao Y, Cao F, Liu H. Radiation-induced Cell Death and Its Mechanisms. Health Phys 2022;123(5):376-86 doi 10.1097/HP.0000000000001601.
19. Britten RA, Warenius HM, White R, Peacock J. BSO-induced reduction of glutathione levels increases the cellular radiosensitivity of drug-resistant human tumor cells. Int J Radiat Oncol Biol Phys 1992;22(4):769-72 doi 10.1016/0360-3016(92)90521-i.
20. Boulares AH, Yakovlev AG, Ivanova V, Stoica BA, Wang G, Iyer S*, et al*. Role of poly(ADP-ribose) polymerase (PARP) cleavage in apoptosis. Caspase 3-resistant PARP mutant increases rates of apoptosis in transfected cells. J Biol Chem 1999;274(33):22932-40 doi 10.1074/jbc.274.33.22932.
21. Shimoni-Sebag A, Abramovich I, Agranovich B, Massri R, Stossel C, Atias D*, et al*. A metabolic switch to the pentose-phosphate pathway induces radiation resistance in pancreatic cancer. Radiother Oncol 2025;202:110606 doi 10.1016/j.radonc.2024.110606.
22. Lee WN, Boros LG, Puigjaner J, Bassilian S, Lim S, Cascante M. Mass isotopomer study of the nonoxidative pathways of the pentose cycle with [1,2-13C2]glucose. Am J Physiol 1998;274(5):E843-51 doi 10.1152/ajpendo.1998.274.5.E843.
23. Sandulache VC, Chen Y, Skinner HD, Lu T, Feng L, Court LE*, et al*. Acute Tumor Lactate Perturbations as a Biomarker of Genotoxic Stress: Development of a Biochemical Model. Mol Cancer Ther 2015;14(12):2901-8 doi 10.1158/1535-7163.MCT-15-0217.
24. Li H, Xu Y, Shi W, Li F, Zeng Q, Yi C. Assessment of alterations in X-ray irradiation-induced DNA damage of glioma cells by using proton nuclear magnetic resonance spectroscopy. Int J Biochem Cell Biol 2017;84:109-18 doi 10.1016/j.biocel.2017.01.010.
25. Day SE, Kettunen MI, Gallagher FA, Hu DE, Lerche M, Wolber J*, et al*. Detecting tumor response to treatment using hyperpolarized 13C magnetic resonance imaging and spectroscopy. Nat Med 2007;13(11):1382-7 doi 10.1038/nm1650.
26. Miloushev VZ, Granlund KL, Boltyanskiy R, Lyashchenko SK, DeAngelis LM, Mellinghoff IK*, et al*. Metabolic Imaging of the Human Brain with Hyperpolarized (13)C

Pyruvate Demonstrates (13)C Lactate Production in Brain Tumor Patients. Cancer Res 2018;78(14):3755-60 doi 10.1158/0008-5472.Can-18-0221.
27. Woitek R, McLean MA, Ursprung S, Rueda OM, Manzano Garcia R, Locke MJ*, et al*. Hyperpolarized Carbon-13 MRI for Early Response Assessment of Neoadjuvant Chemotherapy in Breast Cancer Patients. Cancer Res 2021;81(23):6004-17 doi 10.1158/0008-5472.CAN-21-1499.
28. Ursprung S, Woitek R, McLean MA, Priest AN, Crispin-Ortuzar M, Brodie CR*, et al*. Hyperpolarized (13)C-Pyruvate Metabolism as a Surrogate for Tumor Grade and Poor Outcome in Renal Cell Carcinoma-A Proof of Principle Study. Cancers (Basel) 2022;14(2) doi 10.3390/cancers14020335.
29. Chen HY, Aggarwal R, Bok RA, Ohliger MA, Zhu Z, Lee P*, et al*. Hyperpolarized (13)C-pyruvate MRI detects real-time metabolic flux in prostate cancer metastases to bone and liver: a clinical feasibility study. Prostate Cancer Prostatic Dis 2020;23(2):269-76 doi 10.1038/s41391-019-0180-z.
30. Adjemian S, Oltean T, Martens S, Wiernicki B, Goossens V, Vanden Berghe T*, et al*. Ionizing radiation results in a mixture of cellular outcomes including mitotic catastrophe, senescence, methuosis, and iron-dependent cell death. Cell Death Dis 2020;11(11):1003 doi 10.1038/s41419-020-03209-y.
31. Hao Y, Ren T, Huang X, Li M, Lee JH, Chen Q*, et al*. Rapid phosphorylation of glucose-6-phosphate dehydrogenase by casein kinase 2 sustains redox homeostasis under ionizing radiation. Redox Biol 2023;65:102810 doi 10.1016/j.redox.2023.102810.
32. Wang W, Cui J, Ma H, Lu W, Huang J. Targeting Pyrimidine Metabolism in the Era of Precision Cancer Medicine. Front Oncol 2021;11:684961 doi 10.3389/fonc.2021.684961.
33. Schild T, Keshari KR. Revealing de novo pyrimidine synthesis as a key vulnerability in brain tumors. Cancer Cell 2022;40(12):1457-8 doi 10.1016/j.ccell.2022.10.023.
34. Gwynne WD, Suk Y, Custers S, Mikolajewicz N, Chan JK, Zador Z*, et al*. Cancer-selective metabolic vulnerabilities in MYC-amplified medulloblastoma. Cancer Cell 2022;40(12):1488-502 e7 doi 10.1016/j.ccell.2022.10.009.
35. Shi DD, Savani MR, Levitt MM, Wang AC, Endress JE, Bird CE*, et al*. De novo pyrimidine synthesis is a targetable vulnerability in IDH mutant glioma. Cancer Cell 2022;40(9):939-56 e16 doi 10.1016/j.ccell.2022.07.011.
36. Pal S, Kaplan JP, Nguyen H, Stopka SA, Savani MR, Regan MS*, et al*. A druggable addiction to de novo pyrimidine biosynthesis in diffuse midline glioma. Cancer Cell 2022;40(9):957-72 e10 doi 10.1016/j.ccell.2022.07.012.
37. Zhou W, Yao Y, Scott AJ, Wilder-Romans K, Dresser JJ, Werner CK*, et al*. Purine metabolism regulates DNA repair and therapy resistance in glioblastoma. Nat Commun 2020;11(1):3811 doi 10.1038/s41467-020-17512-x.
38. Kinslow CJ, Chaudhary KR, Upadhyayula PS, Wang TJC, Sun RC, Cheng SK. Purine synthesis as a target for radiation resistance in molecular glioblastoma. J Neurol Sci 2021;425:117439 doi 10.1016/j.jns.2021.117439.
39. Chen AP, Chu W, Gu YP, Cunningham CH. Probing early tumor response to radiation therapy using hyperpolarized [1-^{13}C]pyruvate in MDA-MB-231 xenografts. PLoS One 2013;8(2):e56551 doi 10.1371/journal.pone.0056551.

40. Kawai T, Brender JR, Lee JA, Kramp T, Kishimoto S, Krishna MC*, et al*. Detection of metabolic change in glioblastoma cells after radiotherapy using hyperpolarized (13) C-MRI. NMR Biomed 2021;34(7):e4514 doi 10.1002/nbm.4514.
41. Mair R, Wright AJ, Ros S, Hu DE, Booth T, Kreis F*, et al*. Metabolic Imaging Detects Low Levels of Glycolytic Activity That Vary with Levels of c-Myc Expression in Patient-Derived Xenograft Models of Glioblastoma. Cancer Res 2018;78(18):5408-18 doi 10.1158/0008-5472.CAN-18-0759.
42. Greenwood HE, Witney TH. Latest Advances in Imaging Oxidative Stress in Cancer. J Nucl Med 2021;62(11):1506-10 doi 10.2967/jnumed.120.256974.

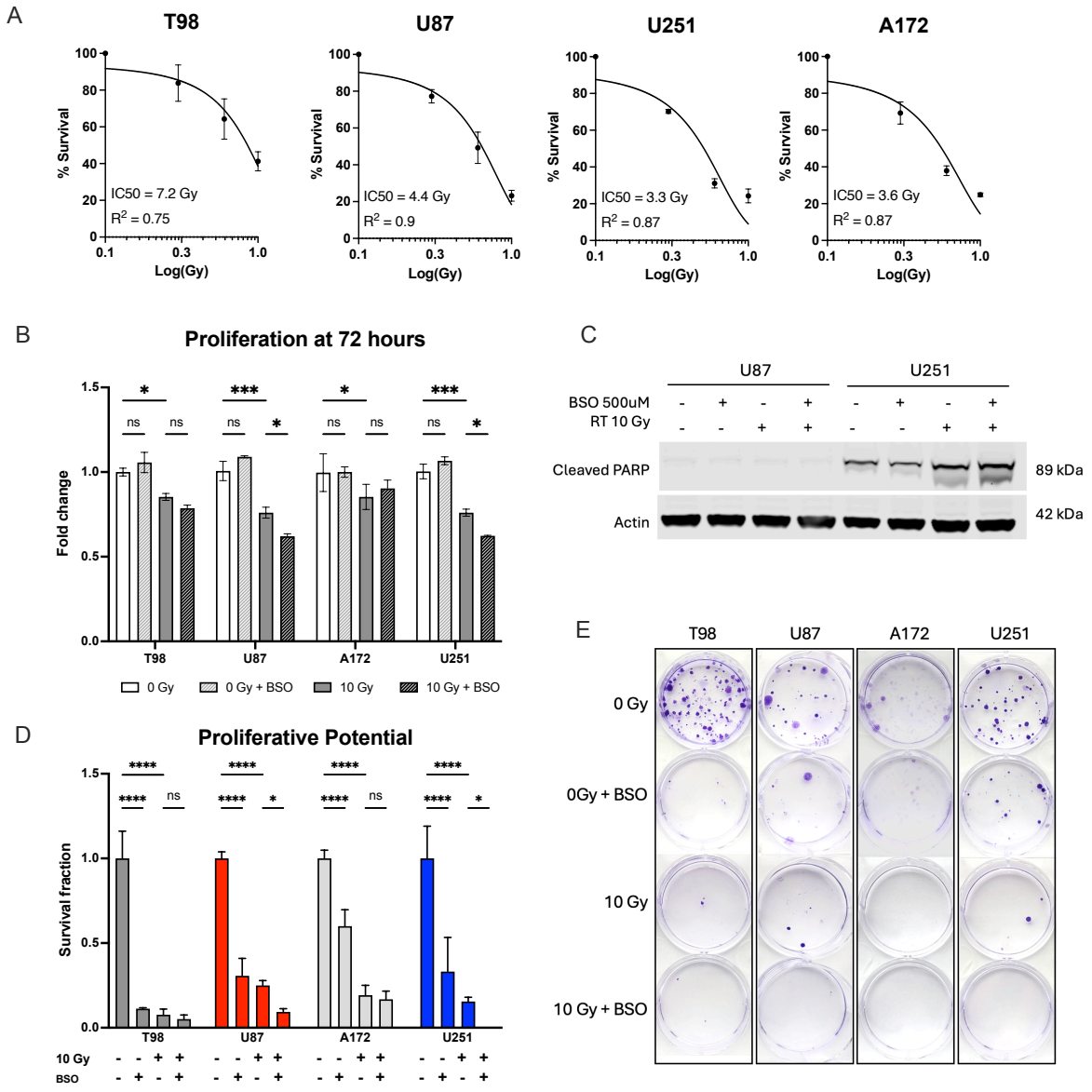

Figure 1: GBM radiation response in vitro. (A) Cell viability 72 hours after treatment with radiation with nonlinear fit with variable slope to obtain an estimate of IC50 and R^2. (B) Proliferation measured by fold change in confluence after 72 hours normalized to untreated control. (C) Western Blot of cleaved-PARP in two GBM lines 48 hours after treatment with either 500 uM BSO for 18 hours, 10 Gy radiation, or both. (D) Clonogenic assays fixed and stained 2 weeks after plating, measuring proliferation potential in each condition. (E) Representative pictures of clonogenic assay wells. Note that A172 did not form as discrete of colonies as the other lines, limiting their visibility. For statistical significance in (B) and (D) 2-way ANOVA performed with significance noted by * symbols.

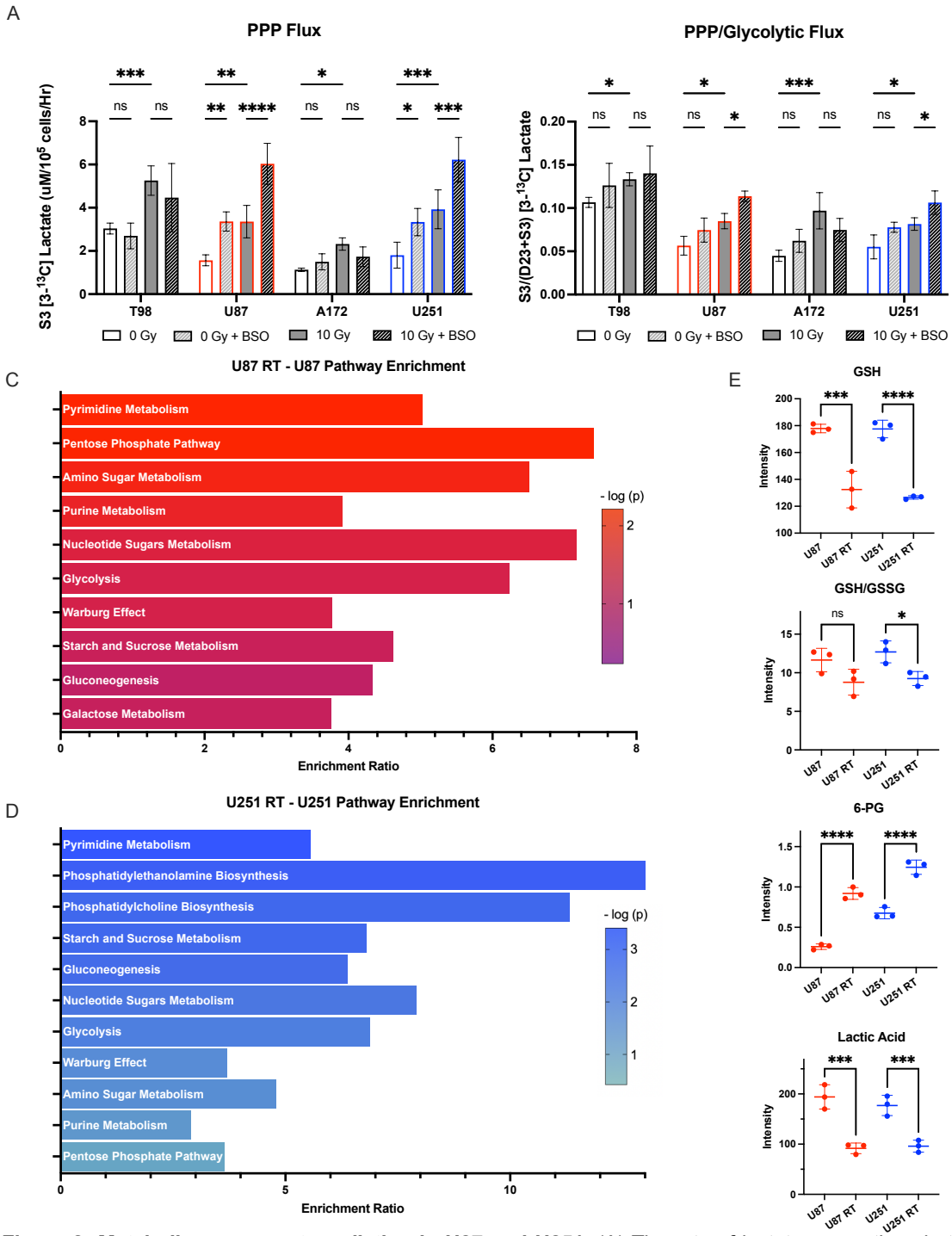

Figure 2: Metabolic response to radiation in U87 and U251. (A) The rate of lactate generation via the Pentose Phosphate Pathway (PPP) is plotted in each cell line treated with 500uM BSO for 18 hours, 10 Gy radiation, or both. (B) PPP/Glycolytic flux expressed as a ratio of M1/(M1+M2) isotopomers. 2-way ANOVA was performed to assess for statistical signficance. (C-D) Pathway Enrichment analyses including all pathways with p>0.1 for U87 and U251s treated with radiation compared to untreated controls of the same cell type. (E) Pool sizes from normalized intensity values of select metabolites. Significance assessed using Welch's ANOVA test.

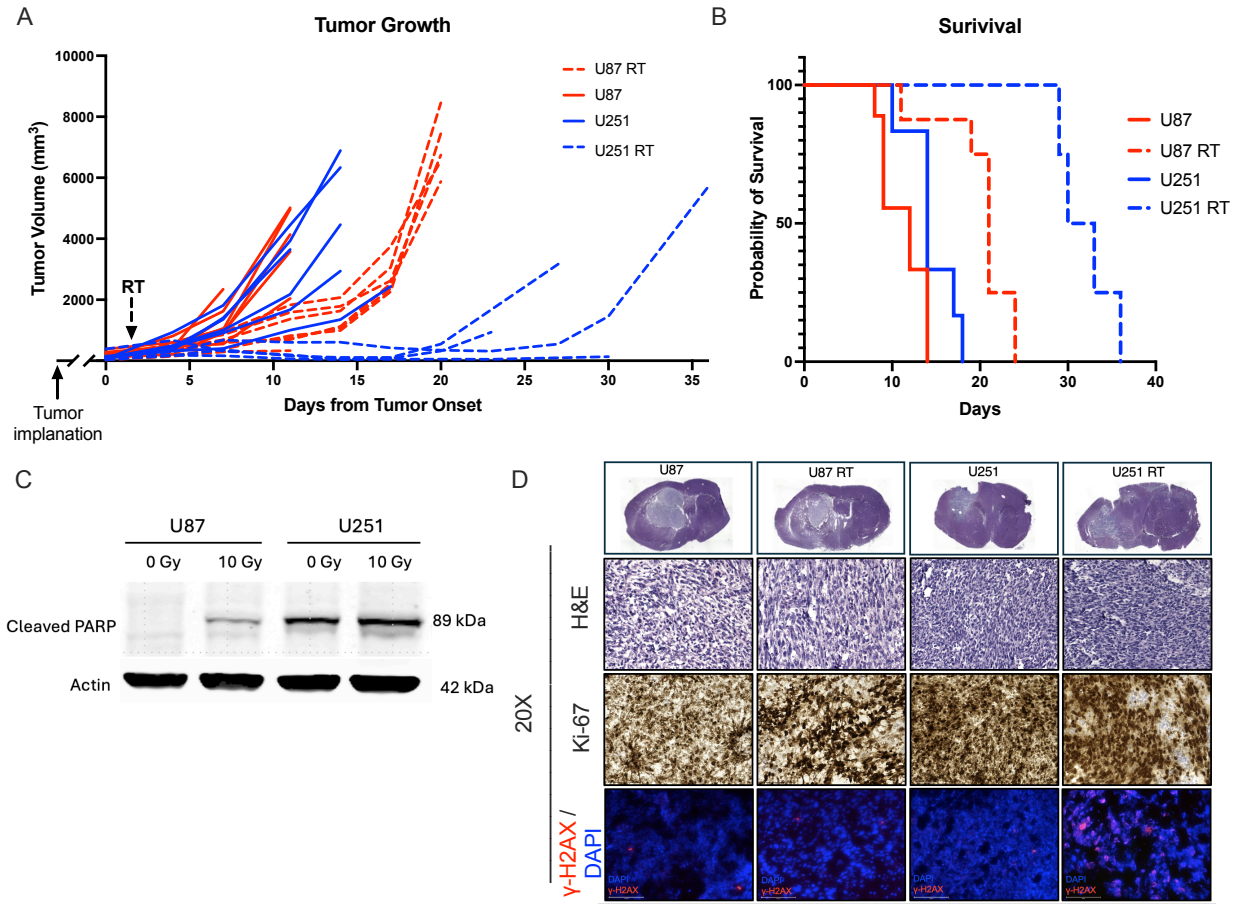

Figure 3: U251s are radiosenstive in vivo compared to U87. (A) Tumor volume curves of mice with U251 or U87 orthotopic xenografts treated with 8Gy radiation or 0 Gy for controls demonstrating a decrement in growth rate of U251s after treatment with radiation. Each line represents one mouse. Mouse numbers per group as follows: U87 = 8, U87 RT = 7, U251 = 6, U251 RT = 4. (B) Kaplan-Meyer survival curve of the same mice from (A), a significantly increased survival benefit was seen in radiated U251s compared to radiated U87s. Time point 0 is date of tumor detection, radiated groups were treated 1-3 days after tumor detection. Log rank test for signfficance between all groups $p<0.0001$, $\chi^2 = 14.52$. (C) Western Blot of cleaved-PARP from tumors 2 days after treatement with radiation. (D) Representative whole brain and 20x images of H&E, ki-67 staining, and γ-H2AX immunoflourescence in flash frozen mouse brains bearing tumors from the same treatment groups.

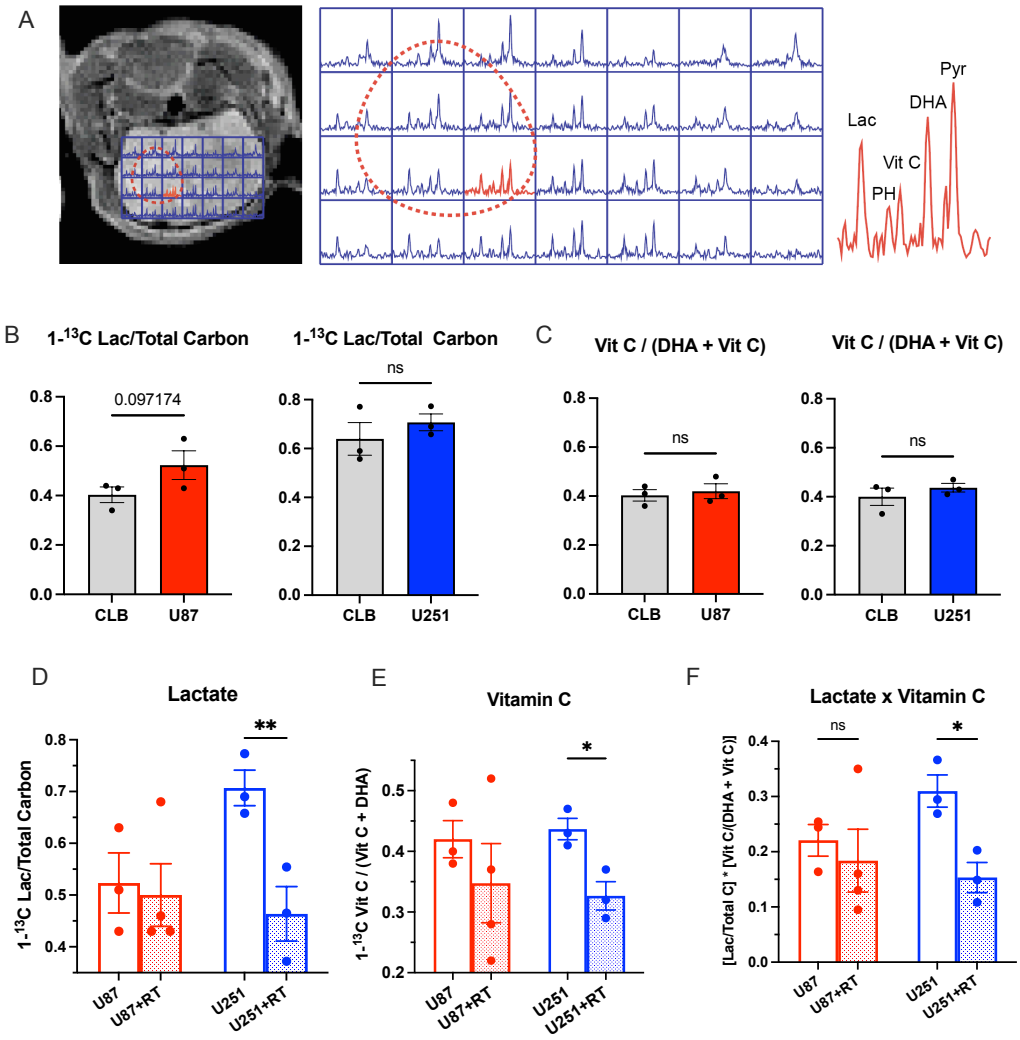

Figure 4. Hyperpolarized dehydroacrobate and pyruvate detects radiation response in GBM. (A) Representative coronal T2-weighted image of U87 tumor brearing mouse brain with 2D CSI spectra acquired 15 seconds after completed injection of HP DHA/PA (40mM/90mM) overlayed, tumor outlined in red dashed line Representative spectra highlighted in red with products and substrates labeled. Pyr: Pyruvate. PH: Pyruvate Hydrate. Lac: Lactate. (B) Product generation comparing tumors with contralateral brain (CLB) in the same mice. Signficance assessed using paired t-tests. (C) Lactate and (D) Vitamin C generation from 4 cohorts of mice (n=3 each except U87 RT which had n=4 mice) demonstrating a decrement in both Vit C and lactate in radioresponsive tumors. (F) Lactate * Vit C may serve as a single biomarker to predict treatment effect in GBM. Signficance in (D-F) assessed using unpaired t-tests comparing treated to untreated groups of the same tumor type.

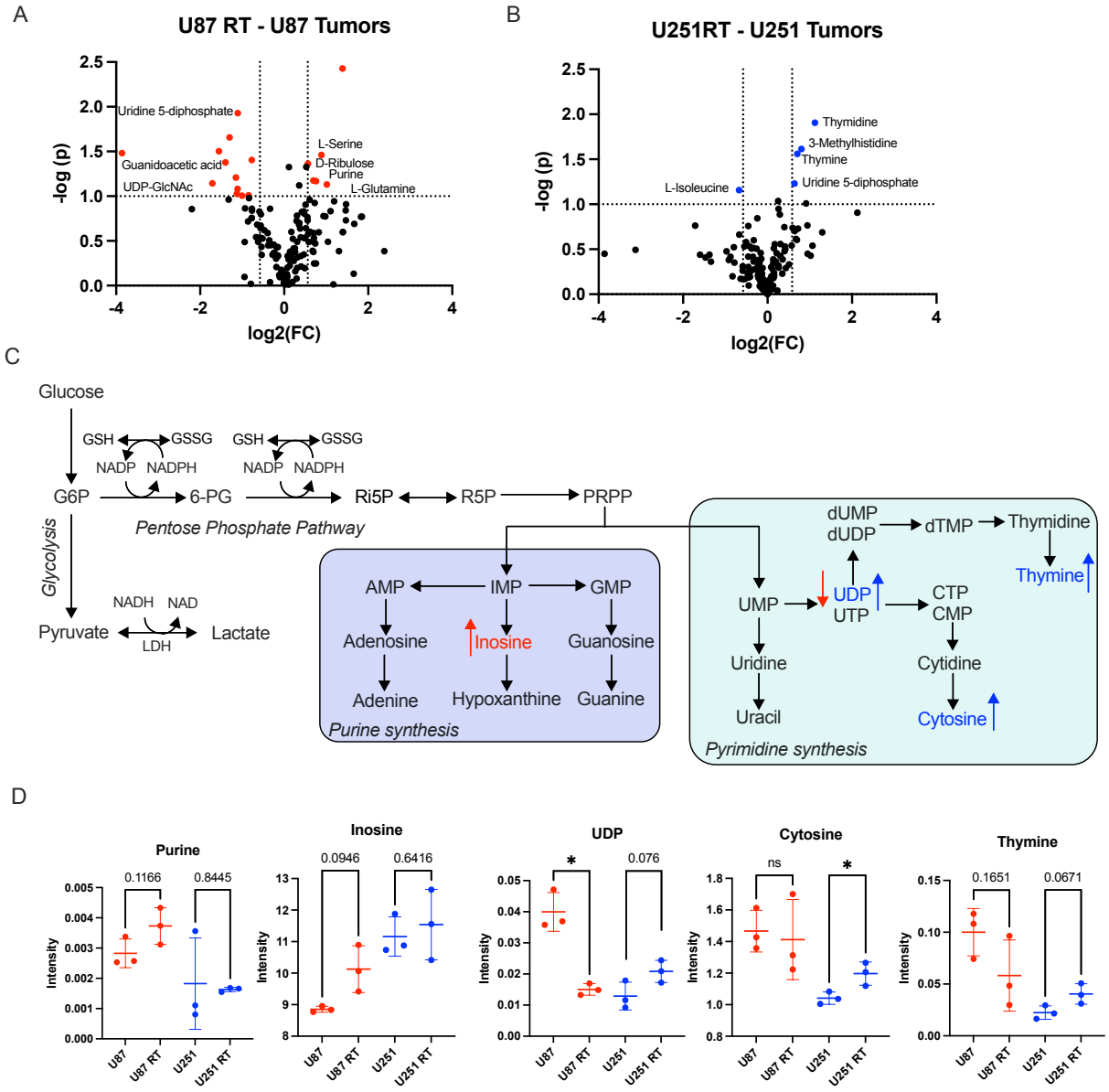

Figure 5: Tumors responding to radiation upregulate pyrmidine synthesis. (A-B) Volcano plots of significant metabolites from flash frozen mouse brain tissue with tumors. Thresholds of p<0.1 and FC >1.5 (<0.66) were used to identify trends towards significance. (C) Figure depicting trends in increased pyrimidines measured in radiosensitive U251s (blue) and increased purine metabolism in radioresistant U87s (red). (D) Pool sizes from normalized intensities of select metabolites. Significance assessed using Welch's ANOVA test.